Journal Pre-proof

Nanoparticle-coupled topical methotrexate can normalize immune responses and induce tissue remodeling in psoriasis

Alaz Özcan, Dilara Sahin, Daniela Impellizzieri, Tuan T. Nguyen, Jürg Hafner, Nikhil Yawalkar, Dennis Kurzbach, Ge Tan, Cezmi A. Akdis, Jakob Nilsson, Onur Boyman, Antonios G.A. Kolios

PII: S0022-202X(19)33373-1

DOI: https://doi.org/10.1016/j.jid.2019.09.018

Reference: JID 2181

To appear in: *The Journal of Investigative Dermatology*

Received Date: 14 March 2019

Revised Date: 3 September 2019

Accepted Date: 12 September 2019

Please cite this article as: Özcan A, Sahin D, Impellizzieri D, Nguyen TT, Hafner J, Yawalkar N, Kurzbach D, Tan G, Akdis CA, Nilsson J, Boyman O, Kolios AGA, Nanoparticle-coupled topical methotrexate can normalize immune responses and induce tissue remodeling in psoriasis, *The Journal of Investigative Dermatology* (2019), doi: https://doi.org/10.1016/j.jid.2019.09.018.

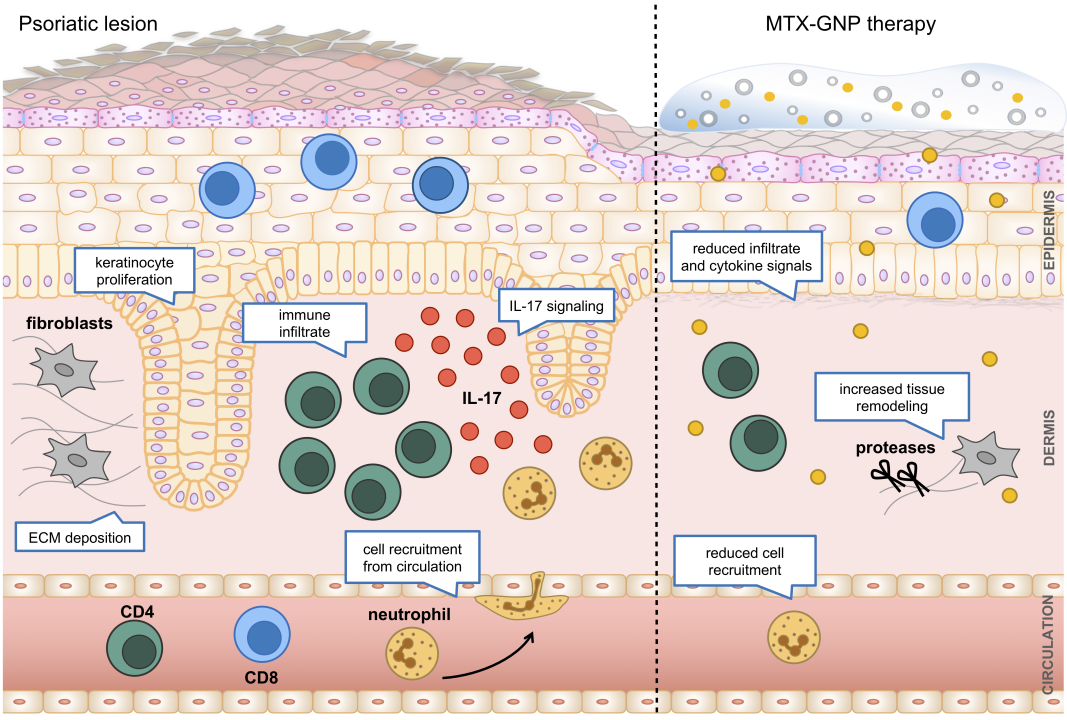
Psoriatic lesion
MTX-GNP therapy
keratinocyte proliferation
fibroblasts
immune infiltrate
IL-17 signaling
IL-17
ECM deposition
cell recruitment from circulation
CD4
CD8
neutrophil
reduced infiltrate and cytokine signals
increased tissue remodeling
proteases
reduced cell recruitment
EPIDERMIS
DERMIS
CIRCULATION

TITLE PAGE

Nanoparticle-coupled topical methotrexate can normalize immune responses and induce tissue remodeling in psoriasis

Alaz Özcan [1], Dilara Sahin [1], Daniela Impellizzieri [1], Tuan T. Nguyen [1], Jürg Hafner [2], Nikhil Yawalkar [3], Dennis Kurzbach [4], Ge Tan [5,8], Cezmi A. Akdis [5,6,7], Jakob Nilsson [1], Onur Boyman [1,7], Antonios G.A. Kolios [1]

Affiliations

[1] Department of Immunology, University Hospital Zurich, Zurich, Switzerland

[2] Department of Dermatology, University Hospital Zurich, Zurich, Switzerland

[3] Department of Dermatology, Inselspital, University Hospital Berne and University of Berne, Berne, Switzerland

[4] University of Vienna, Faculty of Chemistry, Institute of Biological Chemistry, Vienna, Austria

[5] Swiss Institute of Allergy and Asthma Research (SIAF), University of Zurich, Davos, Switzerland

[6] Christine Kühne-Center for Allergy Research and Education, Davos, Switzerland

[7] Faculty of Medicine, University of Zurich, Zurich, Switzerland

[8] Functional Genomics Center Zurich, ETH Zurich/University of Zurich, Zurich, Switzerland

Correspondence

Antonios G.A. Kolios, MD, FAAD, Department of Immunology, University Hospital Zurich and University of Zurich, Gloriastrasse 23, 8091 Zurich, Switzerland. Phone: 0041 – 44 255

89 56. Fax: 0041 – 44 255 13 80. orcid.org/0000-0002-3897-4578. E-Mail: antonios.kolios@usz.ch

ORCIDs:

A. Özcan: 0000-0001-9442-4493, D. Sahin: 0000-0001-7402-8098, D. Impellizzieri: 0000-0003-1045-5896, T.T. Nguyen: 0000-0001-7087-1141, J. Hafner: 0000-0002-4571-1143, N. Yawalkar: 0000-0003-0024-338X, D. Kurzbach: 0000-0001-6455-2136, G. Tan: 0000-0003-0026-8739, C.A. Akdis: 0000-0001-8020-019X, J. Nilsson: 0000-0001-5091-8133, O. Boyman: 0000-0001-8279-5545, A.G.A. Kolios: 0000-0002-3897-4578.

List of Abbreviations

ADAM, A disintegrin and metalloproteinase; ADAMTS, a disintegrin and metalloproteinase with thrombospondin motifs; ALT, alanine transaminase; CLSM, Confocal Laser Scanning Microscopy; DCs, dendritic cells; DEGs, differentially expressed genes; ECM, extracellular matrix; Foxp3, Forkhead box 3; GNP, gold nanoparticle; GO, gene orthology; H&E, hematoxylin eosin; IL, interleukin; IMQ, imiquimod; MTX, methotrexate; NMR, nuclear magnetic resonance; PBMC, peripheral blood mononuclear cells; PN, patient normal-appearing skin; PP, patient psoriatic skin; TCB, topical calcipotriol betamethasone; TNF, tumor necrosis factor; Tregs, regulatory T cells

Short title

Topical MTX-GNP treatment in psoriasis

ABSTRACT

Methotrexate (MTX) is an anti-proliferative drug used for treating inflammatory diseases including psoriasis. Nevertheless, its use in localized therapy is impeded due to poor transdermal penetration.

We show that MTX coupled with gold-nanoparticles (GNPs) demonstrates superior anti-inflammatory efficacy compared to MTX-alone in an imiquimod (IMQ)-induced mouse model, significantly reducing γδ T cells, $CD4^+$ T cells, and neutrophils. Furthermore, it was well tolerated upon systemic and topical administration. In an AGR129 human xenograft mouse model, two-week topical treatment with MTX-GNPs inhibited skin hyperplasia significantly better than topical calcipotriol-betamethasone (TCB) and led to profound tissue remodeling, involving upregulation of extracellular matrix reorganization and downregulation of cornification and keratinization processes. The number of resident T cells in the grafts as well as IL-17 production drastically decreased upon MTX-GNP treatment. While both MTX and MTX-GNPs directly prevented proliferation and induced apoptosis of T cells, suppression of cytokine production was a shared mechanism of GNP and MTX-GNPs.

In conclusion, MTX-GNPs influence immune and stromal components of the skin, leading to potent inhibition of pathogenesis in preclinical psoriasis. MTX-GNPs surpass the efficacy of conventional MTX and standard of care, emerging as a non-steroidal, topical alternative for psoriasis treatment.

INTRODUCTION

Psoriasis is an autoimmune skin disease in which stromal and immune cells, particularly resident and circulating T cells, plasmacytoid dendritic cells (pDCs) and neutrophils, play a significant role in its pathogenesis (Nestle et al., 2009). Targeted biologicals, such as interleukin (IL)-17 blockers, have revolutionized systemic treatment options, but these biologicals are only indicated for moderate-to-severe cases (Kolios et al., 2016). Standard care for mild psoriasis includes topical corticosteroids or topical calcipotriol and betamethasone (TCB) combinations, the former carrying the risk of long-term side effects, including skin atrophy (Samarasekera et al., 2013).

Methotrexate (MTX) is a folate antagonist used as a systemic treatment of psoriasis along with several other inflammatory diseases (Chan and Cronstein, 2002). MTX inhibits cell proliferation, and indirectly leads to intracellular adenosine accumulation, which subsequently impairs activation and migration of leukocytes such as T cells, macrophages, and neutrophils (Chan and Cronstein, 2010). Although there is relative tolerability at standard dose (15mg weekly), adverse reactions may include hepatotoxicity, myelosuppression, infection, and gastrointestinal discomfort (Nast et al., 2017). Localized administration can eliminate systemic side effects; however, to date a topical formulation is not yet commercially available due to the poor skin penetration of MTX (Avasatthi et al., 2016).

Gold nanoparticles (GNPs) facilitate drug delivery across biological barriers and possess immunomodulatory capacities based on their size and surface chemistry (de Araujo et al., 2017). Macrophages and other phagocytic cells take up small sized GNPs which are shown to impair production of proinflammatory cytokines, for example tumor necrosis factor (TNF)-α and IL-6 (Shukla et al., 2005, Tsai et al., 2012). Hence, coupling with GNPs can add an immunomodulatory function to the conjugated drug.

Coupling of MTX to GNPs (MTX-GNPs) was reported to facilitate effective penetration through the human skin barrier in an *ex vivo* system (Bessar et al., 2016). Recently, topical administration of MTX-GNPs was shown to mitigate psoriatic skin inflammation, accompanied by a decrease in proliferation and $CD8^+$ T cell numbers, in a murine model (Fratoddi et al., 2019). However, the effect of MTX-GNPs on immune cells and human skin, as well as the detailed mechanism behind remains unknown.

Here we provide a comprehensive characterization of the anti-inflammatory effect of MTX-GNPs in two pre-clinical models of psoriasis. Using a fully murine and a human xenotransplant model, we account for the biological differences in mouse and human skin. We demonstrate that MTX-GNPs inhibit cell proliferation, cytokine production, and tissue fibrosis, leading to restoration of skin immune-homeostasis.

RESULTS

Systemic MTX-GNPs are efficacious and well tolerated in the Imiquimod (IMQ) model.

IMQ, the active ingredient of ALDARA® cream, is a Toll-like receptor 7 agonist that upon topical administration induces strong psoriasis-like inflammation (van der Fits et al., 2009). Pathogenesis of this model involves neutrophils, dendritic cells (DCs) and γδ T cells, as well as αβ T cells at later stages (Terhorst et al., 2015). In our three-day application setup, shortened and optimized to reduce toxicity, ear skin demonstrates histological features of psoriasis (Supplementary Figure S1a-d). Inflammation is characterized by skin infiltrating $CD45^+$ immune cells, including $CD3^+$ cells and $CD11b^+$ innate immune cells (Supplementary Figure S1e and f). Immune cells in the spleen were primarily unaffected, establishing that the inflammatory phenotype is confined locally (Supplementary Figure S1g and h).

Initially, we evaluated the potency of conventional systemic MTX therapy to resolve IMQ-induced inflammation (Figure 1a). We observed that daily subcutaneous administration was insufficient to diminish ear thickening at tolerable doses of 1mg/kg and 2mg/kg body weight (Figure 1b). With high-dose MTX (5mg/kg daily), ear thickness decreased significantly, however this regimen led to serious toxicity, which was presented as lethargy and severe weight loss (Figure 1b-d). Therefore, inhibition of local inflammation with systemic MTX administration proved intolerable at effective doses.

To enhance *in vivo* efficacy of tolerated MTX doses, MTX was coupled with GNPs (MTX-GNPs). We administered MTX subcutaneously at the tolerable dose of 2mg/kg to avoid toxicity-related complications. MTX-GNPs (2mg/kg MTX, 5.5mg/kg Au) significantly decreased the inflammation-induced ear thickening and immune infiltration (Figure 2e and f). Animals receiving systemic GNPs alone (5.5mg/kg Au) also displayed an improvement of ear inflammation, although the effect was significantly less as compared to MTX-GNPs

(Figure 2e). Systemic MTX-GNPs were well tolerated without causing obvious signs of toxicity, such as lethargy, apathy, severe weight loss, or elevation of serum alanine transaminases (ALT) (Supplementary Figure S2a and b).

Topical MTX-GNPs significantly reduces IMQ-induced inflammation. Topical gel formulations of MTX, GNPs, and MTX-GNPs were generated using the Carbopol 980 carrier. To account for limited drug permeability, selected dosage was six times higher than the systemic administration (Figure 2a). Topical MTX lacked efficacy despite the high dose, whereas ear inflammation subsided significantly upon topical MTX-GNPs ($p=0.0001$, on days 5-7) (Figure 2b). Topical GNPs alone also ameliorated inflammation, however, to a significantly lower extent than topical MTX-GNPs (Figure 2b).

Weight loss and serum ALT levels were comparable among all groups and creatinine levels were below detection limit for all of the tested topical formulation groups (Supplementary Figure S2c and d). Nuclear magnetic resonance (NMR) did not show any traces of MTX, GNP, or MTX-GNPs in the serum of any topical treatment group (Supplementary Figure S3). j

Ear skin treated with MTX or GNPs displayed histological features of IMQ-induced psoriatic phenotype, while the MTX-GNP-treated skin appeared uninflamed, mirroring the untreated condition (Figure 2c). Immunofluorescence staining of skin suggested both the number of infiltrating $CD45^+$ immune cells and IL-17 levels were reduced following MTX-GNP treatment (Figure 2d).

Topical MTX-GNPs strongly suppress key pathogenic immune cells and restore immunological homeostasis. We then characterized the influence of MTX-GNP treatment on skin immune cells, using flow cytometry. Compared to the IMQ group, absolute numbers

of $CD45^+$ leukocytes significantly decreased upon MTX-GNP treatment, mirroring the state in untreated ears (Figure 3a and b). In the myeloid compartment, we observed a pronounced effect on $CD11b^+$cells, namely $Ly6G^+$ neutrophils (Figure 3c and d). Regarding the adaptive compartment, $CD3^+$ T cells in the ears, including γδ and CD4 T cell subsets were highly reduced, while the numbers of $CD8^+$ T cells appeared less responsive at this stage of IMQ-induced inflammation (Figure 3e-g). Neither MTX nor GNPs alone significantly decreased the overall immune cell infiltrate. Only $CD11b^+$ $Ly6G^+$ neutrophils were lower in all treatment groups compared to IMQ alone, with the highest significance for MTX-GNPs (Figure 3d). Absolute numbers of the aforementioned immune cell populations in the spleen remained unaffected by topical therapy (Supplementary Figure S4).

Proliferation of relevant T cell subsets in the ears was assessed by Ki67 positivity. In all experimental groups, γδ T cell proliferation was comparable to the untreated mice, which could be explained by earlier activation kinetics of γδ T cells (Figure 3h). Conversely, $CD4^+$ and $CD8^+$ T cells showed increased proliferative capacity upon IMQ (Figure 3i and j). MTX-GNP treatment significantly decreased the percentage of proliferating $CD4^+$ T cells, while its effect on $CD8^+$ T cells was limited in this setup.

MTX-GNPs inhibit development of psoriasiform lesion in the AGR human xenograft model. The human xenotransplant model is a spontaneous long-term psoriasis model generated by grafting symptomless skin (PN) from a psoriasis patient onto AGR mice, a triple knock-out strain of type I (A) and type II (G) interferon receptors as well as recombination activating gene 2 (R). Transplanted skin develops psoriasis-like phenotype within 4 to 8 weeks, through a pathogenic mechanism mediated by skin-resident human $CD3^+$ T cells within the graft (Boyman et al., 2004, Di Meglio et al., 2016).

Using the AGR model, we assessed the efficiency of MTX-GNPs to resolve human psoriasis in comparison to the standard of care topical bethamethasone calcipotriol (TCB) (Figure 4a). Vaseline-treated grafts displayed histological features of psoriasis on day 35 (Figure 4b, left). The 2-week topical treatment with MTX-GNPs beginning on day 21 significantly reduced acanthosis and papillomatosis scores, whereas TCB treatment showed limited efficacy (Figure 4b and c). While the inflammation in the Vaseline group heightened between day 21 and 35, daily topical administration of MTX-GNP in this time frame arrested further disease progression, to a higher extent than TCB (Supplementary Figure S5d-e).

In the Vaseline treatment group, we observed higher number of $CD45^+$ immune cells, mostly localized in the dermis (Figure 4d and e). This was primarily composed of $CD8^+$ T cells, $CD3^+$ $CD8^-$ Forkhead box P3 $(Foxp3)^+$ regulatory T cells (Tregs), and $CD3^+$ $CD8^-$ $Foxp3^-$ T cells (corresponding to conventional CD4 T cells) (Figure 4f and g), similar to lesional psoriatic (PP) skin biopsies (Supplementary Figure S5a-c). IL-17 was detected in the epidermis and dermis, mostly localized intracellularly, not only in $CD45^+$ immune cells but also in $CD45^-$ non-immune cells. In the TCB or MTX-GNP-treated skin grafts, the cellular infiltrate including IL-17-producing immune cells was significantly reduced or absent (Figure 4d-g). In conclusion, the development of psoriasis and activity of pathogenic immune cells in the grafted human skin was efficaciously blocked by topical MTX-GNP treatment.

MTX-GNPs directly inhibit T cell proliferation and cytokine production.

Further, we evaluated if the anti-inflammatory effect observed upon MTX-GNP treatment in the AGR model is a result of direct suppression of immune cells or an indirect consequence of stromal inhibition. Upon TCR stimulation, human T cells isolated from peripheral blood mononuclear cells (PBMCs) demonstrated increased proliferation and decreased apoptosis, as expected (Figure 5a-c). MTX alone and MTX-GNPs both inhibited proliferation while GNPs

did not have an effect (Figure 5a and b). In line with this, the percentage of apoptotic cells increased upon MTX and MTX-GNPs (Figure 5c). TCR stimulation additionally led to elevated cytokine levels in the culture supernatants. Specifically, Th1 cytokine IFN-γ and Th17 cytokine IL-17A produced significantly higher upon stimulation, while levels of Th2 cytokine IL-4 and Treg cytokine IL-10 remained comparable to unstimulated condition (Figure 5d). MTX alone did not influence cytokine levels in the culture supernatants however, exposure to GNP or MTX-GNPs lowered IFN-γ and, more significantly IL-17A levels.

RNA sequencing reveals significant tissue remodeling in human skin upon topical MTX-GNP application. To identify underlying stromal mechanisms of disease modulation, we performed RNA sequencing (RNA-seq) of PP and PN skin biopsies and AGR skin grafts. RNA-seq revealed 2894 differentially expressed genes (DEGs) and various enriched processes, including cell proliferation, keratinization and immune activation, between the PP and PN biopsies (Supplementary Figure S6a). As expected, chemokines and cytokines implicated in psoriasis pathogenesis (IL-12B, IL-23A, IL17A, IL-1β, IL-36A, CXCL1, and CXCL8) were significantly upregulated in PP skin (Supplementary Figure S6b).

Regarding the AGR grafts, we first performed unbiased Gene Orthology (GO) pathway analysis to reveal treatment-specific effects on biological processes. Within the TCB specific pathways, upregulation of innate and inflammatory responses as well as downregulation of keratinocyte differentiation were the most prominent (Figure 6a). On the other hand, upon MTX-GNPs, pathways related to tissue remodeling and wound healing were upregulated, while cell proliferation processes were downregulated (Figure 6b). Positive regulation of cell

migration and downregulation of keratinization and cornification were the pathways enriched upon both therapies (Figure 6a and b).

We have compared TCB and MTX-GNP treatment to Vaseline-treated controls concerning expression levels of major psoriasis-related cytokines. As expected, treated skin expressed lower levels of pro-inflammatory signals such as S100A8, S1009, IL1B, IL36G, compared to Vaseline control (Figure 6c, highlighted). The effect of TCB treatment on immune-related gene expression was stronger compared to MTX-GNP. However, we have observed a downregulation of TNF, a major driver of psoriatic inflammation, only upon topical MTX-GNP treatment. IL-17A transcript was detectable in the PP skin from the donor patients, however, were below detection limit in PN skin post-transplantation. Therefore, we assessed the expression of these cytokine genes in the post-transplantation skin using real time quantitative PCR (RT-PCR) (Supplementary Figure S6f) and focused our RNA-seq analysis to stromal derived gene expression.

In particular, three gene groups were differentially expressed upon MTX-GNP treatment; keratins, histones and matrix proteases (Figure 6d and e). Keratins were downregulated by both of the treatments, as shown by GO analysis, which explains the curbed epidermal hyperplasia observed in histology (Figure 4b). Histone gene expression was solely decreased in MTX-GNP treated skin. Expression of several matrix proteases was upregulated by both treatments but more significantly in MTX-GNP treatment arm. Overall, the trend of gene expression changes between Vaseline and MTX-GNP reflected the trend between PP and PN skin (Figure 6e).

DISCUSSION

Here, using *in vivo* murine psoriasis-like and human xenograft models, we characterized the therapeutic effect of a topical GNP-coupled MTX formulation, which efficiently mitigates psoriasis development and restores local immune homeostasis. MTX-GNPs reduce proliferation and keratinocyte differentiation and directly act on immune cells by blocking T cell proliferation, promoting apoptosis, and diminishing Th1 and Th17 cytokine production.

In the fully murine IMQ-model, infiltration of both CD11b-expressing innate cells and T cells were reduced upon MTX-GNP treatment with the most prominent effect on the neutrophils, γδ T cells and CD4 T cells. This was accompanied by significant decrease in ear thickness. Importantly, upon both systemic and topical administration, MTX-GNPs were well tolerated at the effective doses.

Although the IMQ-model is quick and involves key effector cells of psoriasis pathogenesis, it has limited translational potential in drug assessment studies, due to vast anatomical and immunological difference between mouse and human skin (Hawkes et al., 2017). Murine skin bears thinner interfollicular epidermis and more hair follicles (Pasparakis et al., 2014), which are crucial determinants of skin composition, such as immune privilege and drug entry sites (Kabashima et al., 2019). Therefore, our xenograft AGR model is more suitable to assess therapeutic efficacy in human psoriatic skin. We demonstrated that psoriatic skin grafts in the AGR model harbored tissue-resident T cell subsets including CD4, CD8 and and regulatory T cells, akin to lesional psoriasis biopsies from patients (PP), underlining the validity of this model for psoriasis research (Boyman et al., 2004, Raeber et al., 2018). A two-week topical MTX-GNP treatment of the human skin grafts prevented the development of psoriatic phenotype and the therapeutic effect was comparable to systemic treatment with anti-TNF-α biologicals, as previously published by our group (Bouchaud et al., 2013,

Boyman et al., 2004). We have shown that 14-day topical treatment with MTX-GNP inhibits psoriasis development in the AGR xenograft model. To our knowledge, no other treatment modality, topical or systemic, has been administered or shown to be effective in a therapeutic setting in this xenotransplantation model. After MTX-GNP treatment, the skin was histologically similar to healthy-appearing non-lesional biopsies (PN) from patients. We demonstrated that the number of above-mentioned immune cells as well as IL-17 levels were significantly reduced compared to psoriatic grafts in the Vaseline control group. RT-PCR analysis of *Il17a* mRNA revealed a similar trend for the transcriptional regulation of IL-17 upon MTX-GNP treatment, which overall suggested an immunomodulatory activity.

Addressing this hypothesis, we used *in vitro* assays and proved that MTX-GNPs directly act on immune cells. In the presence of MTX-GNPs, TCR-stimulated T cells displayed reduced proliferation, impaired cytokine production, and increased apoptosis. While MTX alone also exhibited anti-proliferative and pro-apoptotic effects on T cells, GNPs did not influence cell survival or proliferation, but lowered cytokine production, most significantly IL-17. This indicates that GNPs not only facilitate drug delivery but also enhance anti-inflammatory properties. Our *in vitro* data provides a mechanistic explanation to the *in vivo* effect of GNPs on the IMQ-induced inflammation as well as reduced mRNA and protein levels of IL-17 in the AGR model.

Immune pathology in the human xenograft model was effectively suppressed upon both the TCB and MTX-GNP therapy, while MTX-GNP treated grafts had a significantly lower histopathological disease score. A major function of MTX is to interfere with proliferation of keratinocytes (Weinstein et al., 1990), therefore we hypothesized that suppression of stromal cells can be an important mechanism to explain the difference between the efficacy of the two treatments. In line with this, we demonstrated that MTX-GNPs induced a strong downregulation of anabolic and proliferative processes in skin grafts, while TCB did not.

Additionally, we discovered that topical MTX-GNPs increase the expression of genes involved in extracellular matrix (ECM) breakdown and reorganization, including members of matrix metalloprotease (MMP), a disintegrin and metalloproteinase (ADAM), a disintegrin and metalloproteinase with thrombospondin motifs (ADAMTS) family proteases. It is well-established that ECM buildup and crosstalk with T cells during inflammation can enhance pathogenesis, impede resolution, and foster fibrosis development (Bonnans et al., 2014, Kaisho and Akira, 2003, McFadden et al., 2012, Tsan and Gao, 2004). In the same context, matrix proteases can limit inflammation and tissue fibrosis via ECM degradation. We propose that the enhanced ECM breakdown upon MTX-GNP treatment in the AGR model serves as an additional mechanism to resolve inflammation. In line with this, several *in vivo* studies with diabetic mouse and liver injury rat models have shown that GNPs support wound healing and inhibit fibrosis (Chen et al., 2012, de Carvalho et al., 2018), which provides a possible explanation to tissue-remodeling function of MTX-GNPs. Overall, the therapeutic potency of MTX-GNPs with its multifactorial mode of action exceeds TCB, the standard of care, and MTX in the studied models. Identification of exact mechanisms, both immunomodulatory and stromal, needs further investigation, including clinical assessments.

In conclusion, MTX-GNPs can potentially extend medical practice for the non-steroidal topical treatment of psoriasis and various inflammatory skin disorders, such as *hidradenitis suppurativa*, neutrophil-mediated autoimmune and allergic dermatoses as well as tissue remodeling dysfunctions and keloid formations.

MATERIAL AND METHODS

Animals: C57BL/6 female mice purchased from Charles River Laboratories and AGR129 mice were bred in house homozygously (Boyman et al., 2004). Animals were maintained under specific pathogen-free conditions and all experiments were performed with 8-12-week-old male or female mice.

Compounds: Systemic and topical formulations for MTX, GNPs and MTX-GNPs as well as the carrier Carbopol 980 were provided by Midatech Pharma, Abingdon, United Kingdom.

***In vivo* Imiquimod (IMQ) model:** Ear inflammation was induced by daily application of 60-70mg ALDARA® (5% IMQ, MEDA Pharma, Switzerland) for three consecutive days. Animal wellbeing was evaluated daily with weight measurement by an electronic scale. Daily ear thickness measurements were recorded using a digital micrometer (Mitutoyo®, Japan). Systemic therapies were administered as subcutaneous injections (200µl) and topical therapies as 75µl gel per ear at doses indicated in the figures. After 7 consecutive days of treatments, serum was collected for creatinine and alanine transaminase (ALT) measurements.

AGR model: Keratome biopsies of PN were obtained from consenting patients and were transplanted onto the back of AGR129 mice, as previously described (Boyman et al., 2004). Vaseline (Unilever, US), topical calcipotriol 0.05mg/g and betamethasone dipropionate 0.5mg/g (TCB, Daivobet® gel, Leo Pharma, Denmark), or MTX-GNP gel was topically applied daily onto the grafts from day 21 post-transplantation until termination on day 35. Grafted skin was harvested for histological evaluation and RNA sequencing.

In vitro T cell stimulation: PBMCs from 5 healthy donors were isolated via Ficoll gradient. $CD3^+$ cells were positively selected using Pan T cell Isolation Kit (Miltenyi Biotec Swiss

AG, Switzerland) according to manufacturer's instructions. Isolated T cells were labeled with CellTrace Violet (ThermoFisher Scientific, USA) at 37^0C for 20 minutes. T cells were stimulated for 4 days with anti-CD3 and anti-CD28 antibodies, coated on 96 well Flat bottom plates, in the absence or presence of 100µM of MTX, MTX-GNPs, or GNPs with equivalent MTX or Au concentration. After stimulation, cytokine levels in the supernatants were measured by FACS using Legendplex Human Th Cytokine Panel (Biolegend UK Ltd, United Kingdom) according to manufacturer's instructions. Proliferation and apoptosis assessment of cells were performed by FACS.

FACS: Mouse ears were digested to obtain single cell suspensions (Bouchaud et al., 2013). Single cell suspensions of mouse ears, spleens, or isolated T cells were stained in phosphate buffered saline containing 1% FCS and 2mM EDTA. For the intranuclear staining, cells were fixed and permeabilized after surface staining, according to manufacturer's instructions using the Foxp3/ Transcription Factor Staining kit (eBioscience, ThermoFisher Scientific, USA). For the assessment of apoptosis Fixable Viability Dye eFluor™ 780 (eBioscience, ThermoFisher Scientific, USA, Catalog No: 65-0865-14) was added to the staining mixture of fluorescence-conjugated antibodies. Detailed list of antibodies and providers can be found in the supplementary materials (Table S1).

Histology, Confocal Laser Scanning Microscopy (CLSM): Mouse ears or human skin grafts were embedded in Optimal Cutting Temperature compound (TissueTek, Sakura Finetec, USA) and stored at -80^0C until use. 7µm sections were air dried, fixed with 4% Paraformaldehyde, and stained with H&E based on standard protocols. For immunofluorescence staining, PFA-fixed sections were blocked with PBS containing 5% BSA, 0.1% Triton X prior to antibody staining. Mouse and human skin were stained with primary conjugated or unconjugated antibodies. AlexaFluor647 or AlexaFluor594 conjugated

anti-rabbit antibodies were used as the secondary antibody. Images were acquired on Leica SP8 STED Inverse 3X CLSM, using HC PL APO CS2 20X immersion or 63X oil objectives. Detailed list of antibodies and providers can be found in the supplementary materials (Table S2).

Histology, CLSM quantifications: In human skin samples 10 representative histological fields were selected for the quantification of acanthosis and papillomatosis index (Bouchaud et al., 2013, Fraki et al., 1983). In the AGR xenotransplantation experiments CD3, CD8, CD3+CD8-Foxp3+, CD3+CD8-Foxp3-, CD45+, and CD45+IL17+ cells were independently quantified by two blinded investigators. For each quantified population, 12-16 images of whole graft skin were selected.

RNA sequencing and data analysis: Total RNA was isolated from human punch biopsies, and AGR skin grafts with RNeasy Fibrous Tissue Mini Kit (QIAGEN, Germany). The quality and quantity of RNA was assessed by Tape Station. Library was prepared with SMARTer Stranded Total RNA-Seq Kit - Pico Mammalian Kit (Clontech, USA) and sequenced on a NovaSeq S1 Flowcell in single end 101bp mode. Adapters and low-quality tails were trimmed from reads prior to read alignment. STAR aligner (v2.6.1c) (Dobin et al., 2013) was used to align the RNA-seq dataset to Ensembl genome build GRCh38.p10 (Release 91). Gene expression counts were calculated with feature counts from Bioconductor package Rsubread (v1.32.1) (Liao et al., 2013). A gene was considered expressed if, in at least one comparison group, it had more than 10 counts in more than half of the samples. Differential expressed genes were detected using Bioconductior package DESeq2 (v1.22.1) (Aad et al., 2014). Genes with p-value ≤ 0.01 and log2 fold change ≥ 0.5 were considered significant in this study. Overrepresentation analysis of Gene Ontology categories was performed using Bioconductor package clusterprofiler (v3.10.1).

For Heatmap analysis, mean normalized counts of each group was normalized against the mean normalized counts of the Vaseline control group. The relative expression levels obtained from normalization is expressed as log2. For the floating bar plots, normalized counts of each sample from different groups are shown in log2 scale.

Statistics: Mice were randomly assigned to experimental groups, and results are shown as mean ± SD, or group means, as stated. Comparison of two groups were done by unpaired, parametric two-tailed Student's t test. If multiple groups were statistically compared, unpaired One Way Anova or Two-Way Anova was performed, as reported, followed by Tukey's multiple comparison test. RNA-sequencing data was analyzed using Bioconductior package DESeq2 (Aad et al., 2014).

Study approval: All animal experimentations were approved by the Cantonal Veterinary Office (ZH187/16) and performed in accordance with the Swiss Animal Laws. Ethical approval for human samples (skin grafts, biopsies, and blood) was obtained by the Cantonal Ethics Committee Zurich (2018-01413) and performed in accordance. All patients has given written, informed consent before their participation in the study.

DATA AVAILABILITY

Datasets related to this article can be found at Gene Expression Omnibus database (GEO GSE126066), hosted at NCBI.

CONFLICT OF INTERESTS

The authors state no conflict of interest.

ACKNOWLEDGEMENTS

We thank Martina McAteer, Tom Coulter and Yao Ding (Midatech Pharma, Abingdon, United Kingdom) for providing MTX formulations and Functional Genomics Center Zurich (FGCZ) for their technical support in RNA sequencing. We specially thank Catherine Crowley-Kühn for reading and editing the manuscript.

This work was funded by Swiss National Science Foundation (#310030-172978; to O.B.), the Hochspezialisierte Medizin Schwerpunkt Immunologie (HSM-2-Immunologie; to O.B.), the Clinical Research Priority Program of the University of Zurich for the CRPP CYTIMM-Z (to O.B.), and the University Hospital Zurich.

AUTHOR CONTRIBUTIONS (in accordance with CRediT Taxonomy)

Conceptualization: O. Boyman, A.G.A Kolios.

Data curation: A. Özcan, A.G.A Kolios.

Formal analysis: A. Özcan, D. Kurzbach, G. Tan.

Funding acquisition: O. Boyman, A.G.A Kolios.

Investigation: A. Özcan, D. Sahin, T.T. Nguyen, D. Impellizzieri, D. Kurzbach, G. Tan.

Methodology: A. Özcan, A.G.A Kolios.

Project administration: A.G.A Kolios.

Resources: A. Özcan, J. Hafner, N. Yawalkar, O. Boyman, A.G.A Kolios.

Software: G. Tan, D. Kurzbach.

Supervision: A.G.A Kolios.

Validation: A. Özcan, D. Kurzbach, G. Tan.

Visualization: A. Özcan.

Writing-original draft: A. Özcan, D. Sahin, A.G.A Kolios.

Writing-review and editing: J. Hafner, N. Yawalkar, D. Kurzbach, C.A. Akdis, J. Nilsson, O. Boyman, A.G.A Kolios.

REFERENCES

Aad G, Abbott B, Abdallah J, Abdel Khalek S, Abdinov O, Aben R, et al. Search for scalar diphoton resonances in the mass range 65-600 GeV with the ATLAS detector in pp collision data at radicals=8 TeV. Phys Rev Lett 2014;113(17):171801.

Avasatthi V, Pawar H, Dora CP, Bansod P, Gill MS, Suresh S. A novel nanogel formulation of methotrexate for topical treatment of psoriasis: optimization, in vitro and in vivo evaluation. Pharm Dev Technol 2016;21(5):554-62.

Bessar H, Venditti I, Benassi L, Vaschieri C, Azzoni P, Pellacani G, et al. Functionalized gold nanoparticles for topical delivery of methotrexate for the possible treatment of psoriasis. Colloids Surf B Biointerfaces 2016;141:141-7.

Bonnans C, Chou J, Werb Z. Remodelling the extracellular matrix in development and disease. Nat Rev Mol Cell Biol 2014;15(12):786-801.

Bouchaud G, Gehrke S, Krieg C, Kolios A, Hafner J, Navarini AA, et al. Epidermal IL-15Ralpha acts as an endogenous antagonist of psoriasiform inflammation in mouse and man. J Exp Med 2013;210(10):2105-17.

Boyman O, Hefti HP, Conrad C, Nickoloff BJ, Suter M, Nestle FO. Spontaneous development of psoriasis in a new animal model shows an essential role for resident T cells and tumor necrosis factor-alpha. J Exp Med 2004;199(5):731-6.

Chan ES, Cronstein BN. Molecular action of methotrexate in inflammatory diseases. Arthritis Res 2002;4(4):266-73.

Chan ES, Cronstein BN. Methotrexate--how does it really work? Nat Rev Rheumatol 2010;6(3):175-8.

Chen SA, Chen HM, Yao YD, Hung CF, Tu CS, Liang YJ. Topical treatment with anti-oxidants and Au nanoparticles promote healing of diabetic wound through receptor for advance glycation end-products. Eur J Pharm Sci 2012;47(5):875-83.

de Araujo RFJ, de Araujo AA, Pessoa JB, Freire Neto FP, da Silva GR, Leitao Oliveira AL, et al. Anti-inflammatory, analgesic and anti-tumor properties of gold nanoparticles. Pharmacol Rep 2017;69(1):119-29.

de Carvalho TG, Garcia VB, de Araujo AA, da Silva Gasparotto LH, Silva H, Guerra GCB, et al. Spherical neutral gold nanoparticles improve anti-inflammatory response, oxidative stress and fibrosis in alcohol-methamphetamine-induced liver injury in rats. Int J Pharm 2018;548(1):1-14.

Di Meglio P, Villanova F, Navarini AA, Mylonas A, Tosi I, Nestle FO, et al. Targeting CD8(+) T cells prevents psoriasis development. J Allergy Clin Immunol 2016;138(1):274-6 e6.

Dobin A, Davis CA, Schlesinger F, Drenkow J, Zaleski C, Jha S, et al. STAR: ultrafast universal RNA-seq aligner. Bioinformatics 2013;29(1):15-21.

Fraki JE, Briggaman RA, Lazarus GS. Transplantation of psoriatic skin onto nude mice. J Invest Dermatol 1983;80 Suppl:31s-5s.

Fratoddi I, Benassi L, Botti E, Vaschieri C, Venditti I, Bessar H, et al. Effects of topical methotrexate loaded gold nanoparticle in cutaneous inflammatory mouse model. Nanomedicine 2019.

Hawkes JE, Gudjonsson JE, Ward NL. The Snowballing Literature on Imiquimod-Induced Skin Inflammation in Mice: A Critical Appraisal. J Invest Dermatol 2017;137(3):546-9.

Kabashima K, Honda T, Ginhoux F, Egawa G. The immunological anatomy of the skin. Nat Rev Immunol 2019;19(1):19-30.

Kaisho T, Akira S. Regulation of dendritic cell function through toll-like receptors. Curr Mol Med 2003;3(8):759-71.

Kolios AG, Yawalkar N, Anliker M, Boehncke WH, Borradori L, Conrad C, et al. Swiss S1 Guidelines on the Systemic Treatment of Psoriasis Vulgaris. Dermatology 2016;232(4):385-406.

Liao Y, Smyth GK, Shi W. The Subread aligner: fast, accurate and scalable read mapping by seed-and-vote. Nucleic Acids Res 2013;41(10):e108.

McFadden J, Fry L, Powles AV, Kimber I. Concepts in psoriasis: psoriasis and the extracellular matrix. Br J Dermatol 2012;167(5):980-6.

Nast A, Spuls PI, van der Kraaij G, Gisondi P, Paul C, Ormerod AD, et al. European S3-Guideline on the systemic treatment of psoriasis vulgaris - Update Apremilast and Secukinumab - EDF in cooperation with EADV and IPC. J Eur Acad Dermatol Venereol 2017;31(12):1951-63.

Nestle FO, Kaplan DH, Barker J. Psoriasis. N Engl J Med 2009;361(5):496-509.

Pasparakis M, Haase I, Nestle FO. Mechanisms regulating skin immunity and inflammation. Nat Rev Immunol 2014;14(5):289-301.

Raeber ME, Zurbuchen Y, Impellizzieri D, Boyman O. The role of cytokines in T-cell memory in health and disease. Immunol Rev 2018;283(1):176-93.

Samarasekera EJ, Sawyer L, Wonderling D, Tucker R, Smith CH. Topical therapies for the treatment of plaque psoriasis: systematic review and network meta-analyses. Br J Dermatol 2013;168(5):954-67.

Shukla R, Bansal V, Chaudhary M, Basu A, Bhonde RR, Sastry M. Biocompatibility of gold nanoparticles and their endocytotic fate inside the cellular compartment: a microscopic overview. Langmuir 2005;21(23):10644-54.

Terhorst D, Chelbi R, Wohn C, Malosse C, Tamoutounour S, Jorquera A, et al. Dynamics and Transcriptomics of Skin Dendritic Cells and Macrophages in an Imiquimod-Induced, Biphasic Mouse Model of Psoriasis. J Immunol 2015;195(10):4953-61.

Tsai CY, Lu SL, Hu CW, Yeh CS, Lee GB, Lei HY. Size-dependent attenuation of TLR9 signaling by gold nanoparticles in macrophages. J Immunol 2012;188(1):68-76.

Tsan MF, Gao B. Endogenous ligands of Toll-like receptors. J Leukoc Biol 2004;76(3):514-9.

van der Fits L, Mourits S, Voerman JS, Kant M, Boon L, Laman JD, et al. Imiquimod-induced psoriasis-like skin inflammation in mice is mediated via the IL-23/IL-17 axis. J Immunol 2009;182(9):5836-45.

Weinstein GD, Jeffes E, McCullough JL. Cytotoxic and immunologic effects of methotrexate in psoriasis. J Invest Dermatol 1990;95(5 Suppl):49S-52S.

FIGURE LEGENDS

Figure 1. Efficacy of systemic MTX and MTX-GNP in the IMQ model. (**a**) Experimental scheme. (**b**) Left, representative plot of two independent experiments depicting ear thickness of untreated (n = 4), IMQ-treated (n = 5), and systemic MTX-therapy (n = 4 for 1mg/kg, 2mg/kg, 5mg/kg) receiving animals. Right, corresponding statistical analysis. (**c** and **d**) Weight changes of different treatment groups in the MTX dose escalation (n = 4-5) calculated as % weight change from pretreatment weight and recorded daily (**c**) and plotted for day 7 (**d**). (**e**) Left, ear thickness of untreated (n = 8), IMQ-treated (n = 9), and systemic therapy (n = 12 for MTX, n = 8 for GNP, and n = 7 for MTX-GNP) receiving animals. Right, corresponding statistical analysis. (**f**) Quantification of $CD45^+$ (**c**), $CD3^+$ (**d**) and $CD11b^+$ (**e**) cell populations in the ears of untreated (n = 10-11), IMQ-treated (n = 11), and systemic MTX (n = 7-9), GNP (n = 4-7), or MTX-GNP (n = 4-6) therapy receiving animals on day 7. Data are pooled from 4 (**b-d**) or 3 (**e** and **f**) independent experiments and shown as mean ± SD (**b-e**) or mean (**f**). Data are analyzed by either One-Way (**d** and **f**) or Two-Way Anova (**b, c** and **e**). ns = non-significant, * $p<0.05$, ** $p<0.01$, *** $p<0.001$, **** $p<0.0001$.

Figure 2. Efficacy of topical MTX-GNP in the IMQ model. (**a**) Experimental scheme. (**b**) Left, ear thickness of untreated (n = 8), IMQ-treated (n = 12), and topical therapy (n = 7 for Carbopol 980 gel carrier, n = 8 for MTX gel, n = 9 for GNP, and n = 9 for MTX-GNP) receiving animals. Right, corresponding statistical analysis. (**c-d**) Representative H&E (**c**) and immunofluorescence (**d**) staining of ear skin harvested on day 7. (**c**) Scale bar = 200µm. (**d**) CD45 (red), IL-17 (green), and DAPI (blue). Scale bar = 100µm. Data are pooled from 3 independent experiments and shown as mean ± SD. Data are analyzed by Two-Way Anova. ns = non-significant, * $p<0.05$, ** $p<0.01$, *** $p<0.001$, **** $p<0.0001$.

Figure 3. Flow cytometry analysis of skin immune landscape upon topical therapies on day 7. (**a**) Representative pseudocolor plots and (**b**) quantification of $CD45^+$ cell population in ears. (**c**) Quantification of total $CD11b^+$ cell populations and (**d**) $Ly6G^+$ and $Ly6G^-$ cell composition of

$CD11b^+$ cells. (**e**) Quantification of $CD3^+$ cell population and (**f**) αβ and γδ T cell composition of $CD3^+$ T cells. (**g**) Quantification of $CD4^+$ and $CD8^+$ T cell composition of αβ $CD3^+$ T cells. (**h-j**) $Ki67^+$ cell percentage of $\gamma\delta^+$ (**h**), $CD4^+$ (**i**) and $CD8^+$ (**j**) T cell subsets. Data are pooled from 3 independent experiments and represented as mean. Data are analyzed by either One-Way (**b, c, e** and **h-j**) or Two-Way Anova (**d, f** and **g**). ns = non-significant.

Figure 4. Effect of topical MTX-GNP on the AGR model of psoriasis. (**a**) Experimental scheme. (**b**) Representative H&E staining of skin grafts harvested on day 35. Scale bar = 100µm. (**c**) Quantification of acanthosis (left) and papillomatosis index (right) upon Vaseline (n = 4), TCB (n = 5), or MTX-GNP (n = 5) treatments. (**d-g**) Representative immunofluorescence staining of Vaseline, TCB, and MTX-GNP treated transplant skin on day 35. (**d**) CD45 (green, arrowhead), IL-17 (magenta, asterisk), and DAPI (blue). (**e**) Quantification of $CD45^+$ and $CD45^+IL\text{-}17^+$ cells from the immunofluorescence images. (**f**) CD3 (green, arrowhead), Foxp3 (magenta, asterisk), CD8 (red, arrow), and DAPI (blue). (**g**) Quantification of $CD3^+$, $CD3^+CD8^+$, $CD3^+CD8^-Foxp3^+$ and $CD3^+CD8^-Foxp3^-$ cells from the immunofluorescence images. Bottom images display the indicated squares in higher magnification. Scale bar = 100µm (top), and 50µm (bottom). Data are pooled from 3 independent experiments and shown as mean. Data are analyzed by One-Way Anova. ns = non-significant.

Figure 5. MTX-GNPs directly inhibit T cell proliferation and cytokine production. (**a**) Representative histograms of CTV staining of $CD4^+$ and $CD8^+$ T cells following 4-day culture with media or with coated anti-CD3, anti-CD28 stimulation together with media, MTX, GNP or MTX-GNP. (**b** and **c**) Percentage of (**b**) proliferating and (**c**) apoptotic $CD3^+$, $CD4^+$ and $CD8^+$ T cells at day 4 upon indicated culture conditions. (**d**) Concentration of IFN-γ, IL-17A, IL-4 and IL-10 in the supernatant of cultured T cells.

Figure 6. Transcriptomic profile of the psoriatic skin grafts. (**a** and **b**) Enriched biological processes upon TCB (**a**) or MTX-GNP (**b**) treatment compared to Vaseline. Red bars: upregulation, blue bars: downregulation, filled bars: common pathways between two therapies. (**c** and **d**) DEGs in TCB and MTX-GNP treatment normalized to Vaseline (**c**) immune related genes and (**d**) gene sets involved in keratin synthesis, histone modification, and matrix proteases production. (**e**) Normalized expression of selected DEGs from Vaseline, TCB and MTX-GNP treated grafts and, PP and PN skin biopsies.

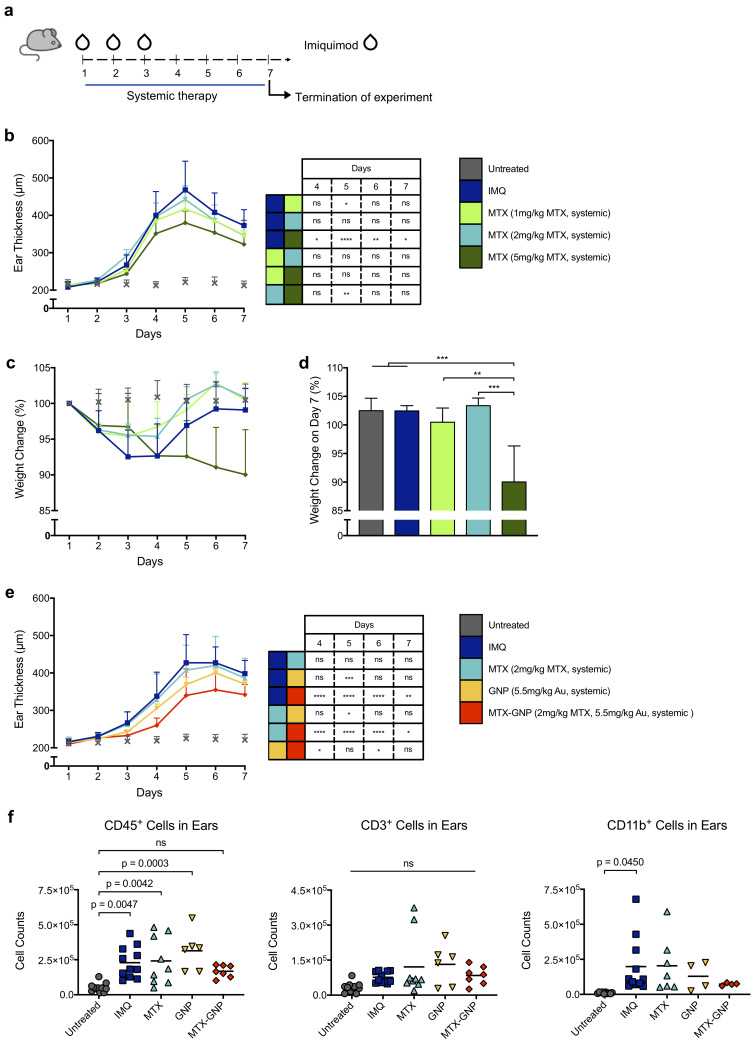

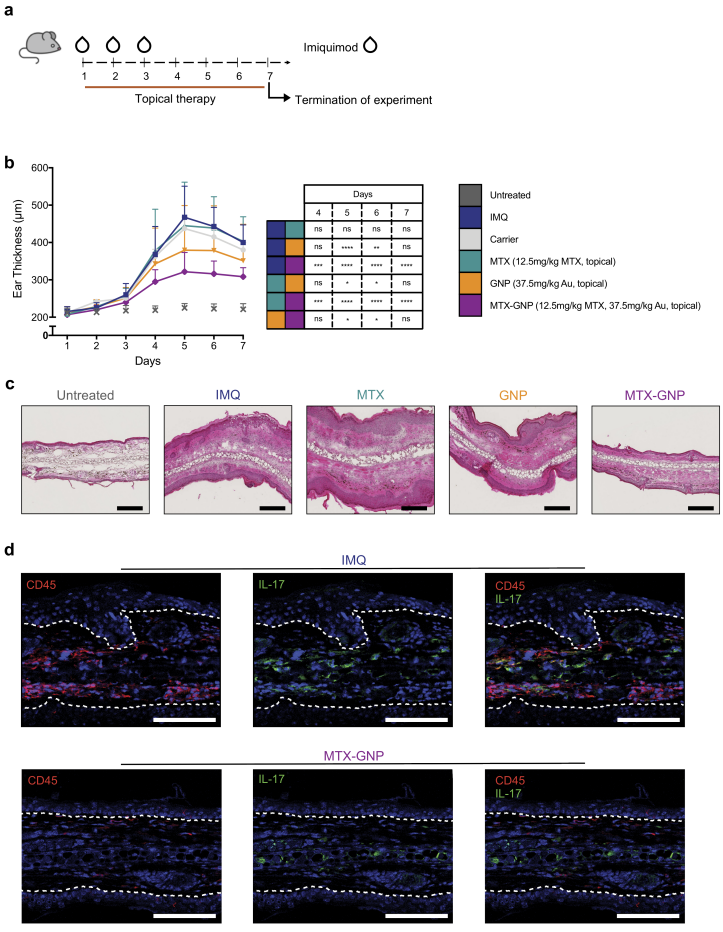
a
Imiquimod
1 2 3 4 5 6 7
Topical therapy
Termination of experiment
b
Ear Thickness (μm)
600
500
400
300
200
0
1 2 3 4 5 6 7
Days
Days
4 5 6 7
ns ns ns ns
ns **** ** ns
*** **** **** ****
ns * * ns
*** **** **** ****
ns * * ns
Untreated
IMQ
Carrier
MTX (12.5mg/kg MTX, topical)
GNP (37.5mg/kg Au, topical)
MTX-GNP (12.5mg/kg MTX, 37.5mg/kg Au, topical)
c
Untreated
IMQ
MTX
GNP
MTX-GNP
d
IMQ
CD45
IL-17
CD45
IL-17
MTX-GNP
CD45
IL-17
CD45
IL-17

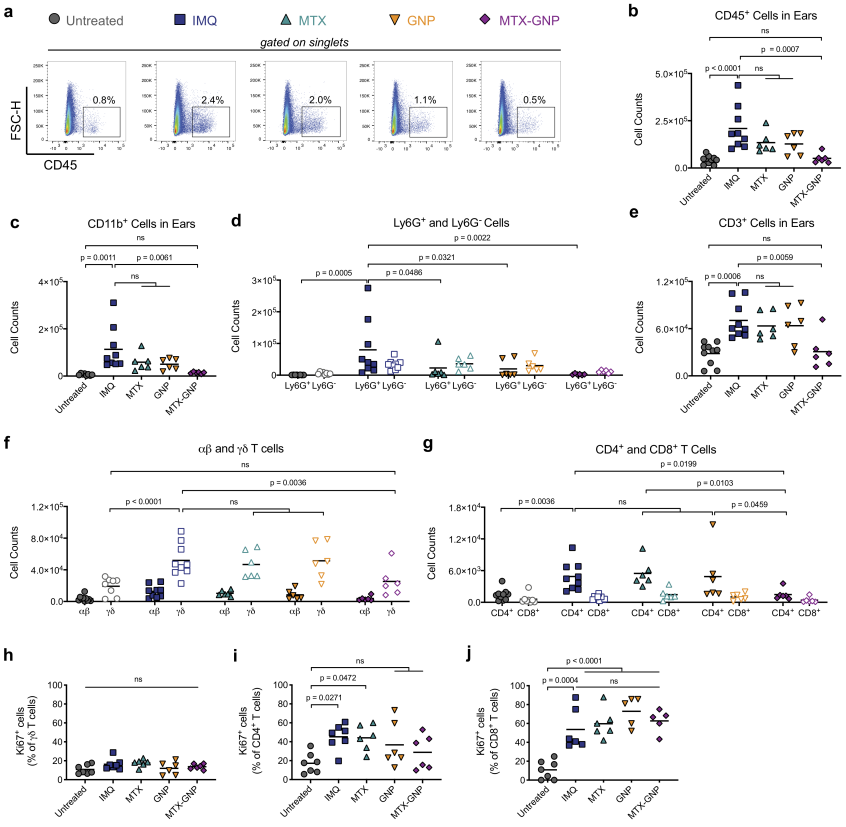

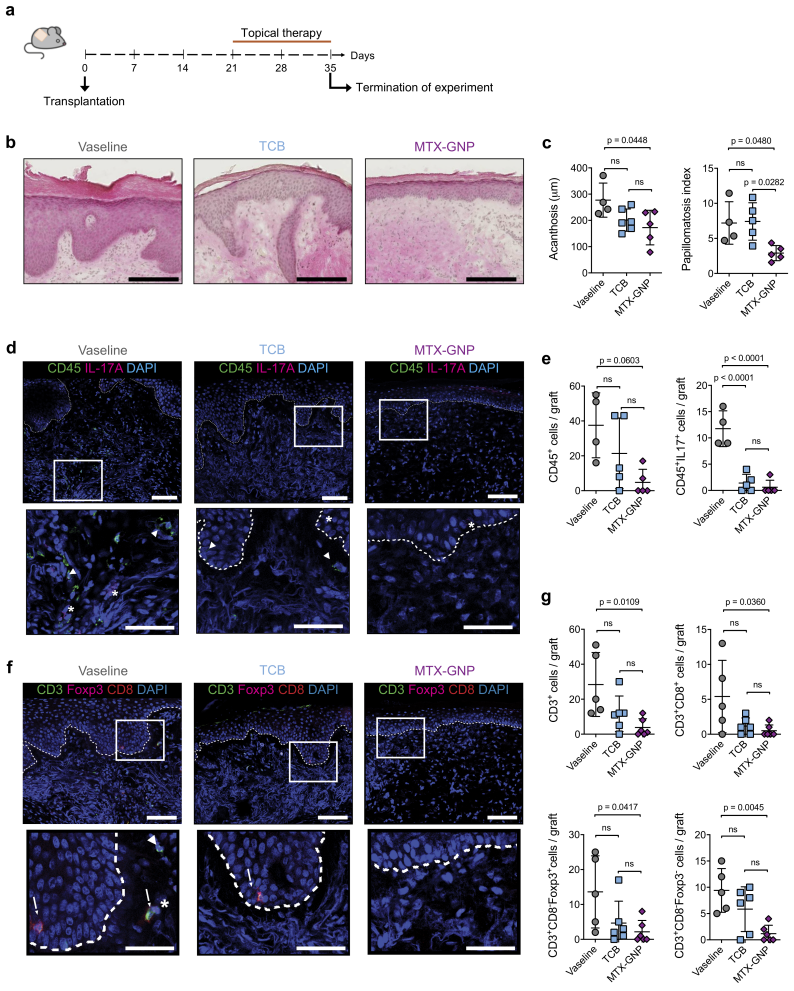
a
Topical therapy
0
7
14
21
28
35
Days
Transplantation
Termination of experiment
b
Vaseline
TCB
MTX-GNP
c
p = 0.0448
ns
ns
Acanthosis (μm)
p = 0.0480
ns
p = 0.0282
Papillomatosis index
Vaseline
TCB
MTX-GNP
d
Vaseline
TCB
MTX-GNP
CD45 IL-17A DAPI
e
p = 0.0603
ns
ns
CD45+ cells / graft
p < 0.0001
p < 0.0001
ns
CD45+IL17+ cells / graft
f
Vaseline
TCB
MTX-GNP
CD3 Foxp3 CD8 DAPI
g
p = 0.0109
ns
ns
CD3+ cells / graft
p = 0.0360
ns
ns
CD3+CD8+ cells / graft
p = 0.0417
ns
ns
CD3+CD8-Foxp3+cells / graft
p = 0.0045
ns
ns
CD3+CD8-Foxp3- cells / graft

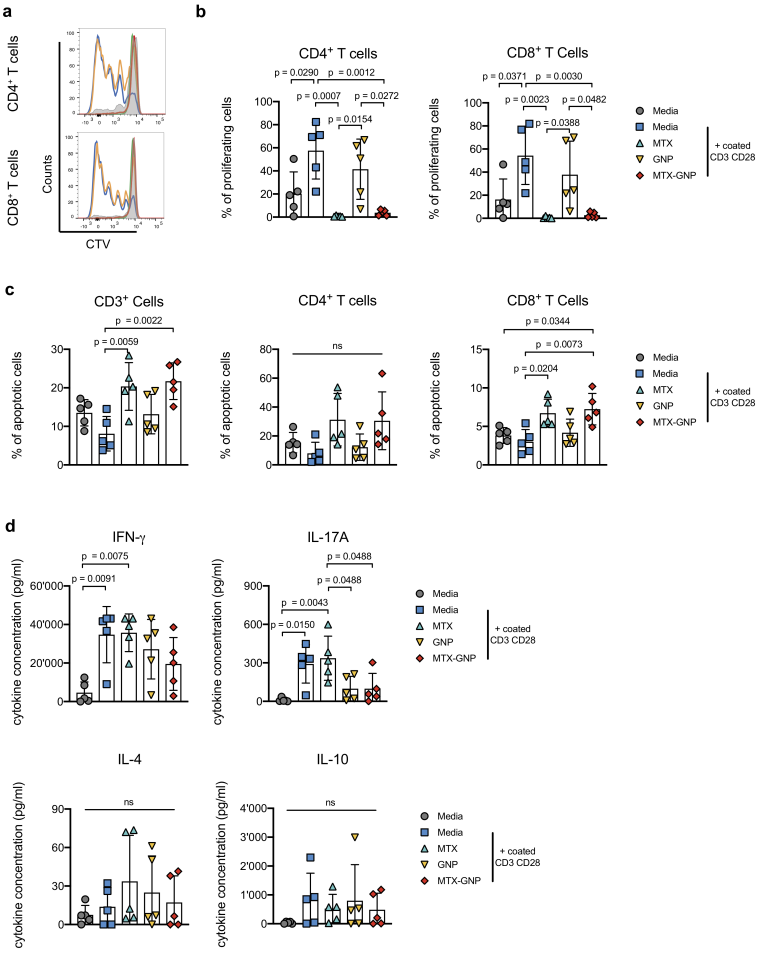
a
CD4+ T cells
CD8+ T cells
Counts
CTV
b
CD4+ T cells
CD8+ T Cells
% of proliferating cells
p = 0.0290
p = 0.0012
p = 0.0007
p = 0.0272
p = 0.0154
p = 0.0371
p = 0.0030
p = 0.0023
p = 0.0482
p = 0.0388
Media
Media
MTX
GNP
MTX-GNP
+ coated CD3 CD28
c
CD3+ Cells
CD4+ T cells
CD8+ T Cells
% of apoptotic cells
p = 0.0022
p = 0.0059
ns
p = 0.0344
p = 0.0073
p = 0.0204
d
IFN-γ
IL-17A
IL-4
IL-10
cytokine concentration (pg/ml)
p = 0.0075
p = 0.0091
p = 0.0488
p = 0.0488
p = 0.0043
p = 0.0150
ns
ns

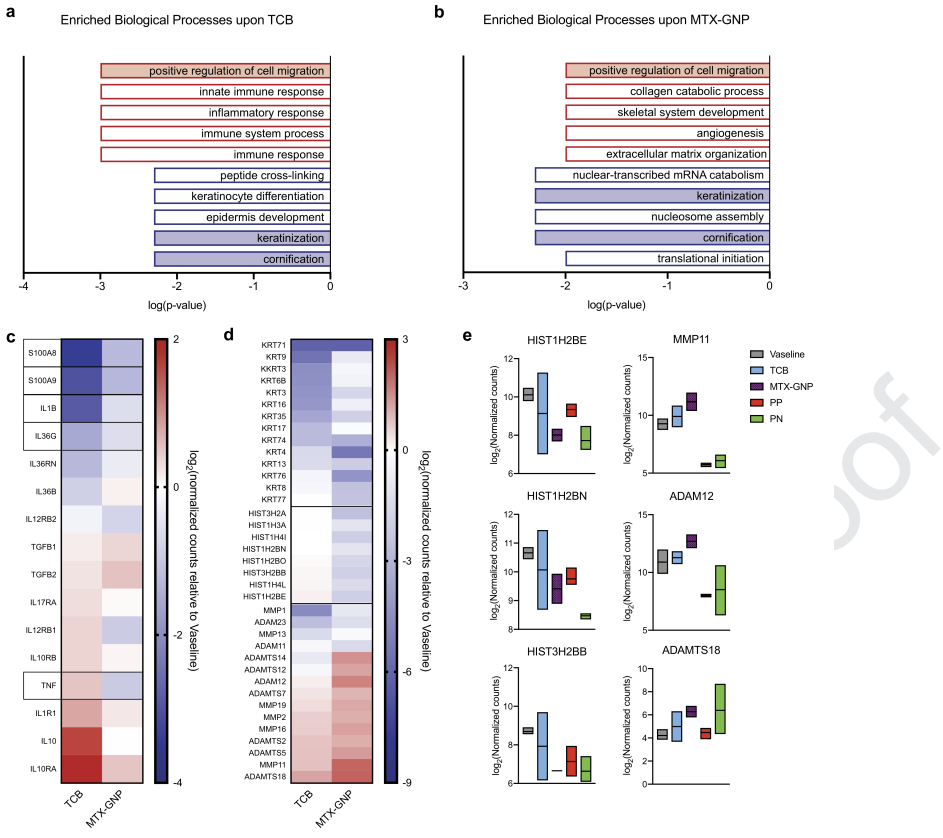

SUPPLEMENTARY FIGURE LEGENDS

Supplementary Figure S1. The three-day IMQ model. (**a**) Experimental scheme. (**b**) Representative H&E staining of untreated (left) and IMQ-treated (right) ear skin on day 7. Scale bar = 100µm. (**c**) Top, ear thickness of untreated (n = 8) and IMQ-treated (n = 12) animals. Bottom, corresponding statistical analysis. (**d**) Top, weight changes of untreated (n = 8) or IMQ-treated (n = 12) animals were calculated as % weight change from pretreatment weight and recorded daily. Bottom, statistical analysis of weight differences of the two groups between days 3-7. (**e-h**) $CD45^+$, $CD3^+$ and $CD11b^+$ cells in the ears (**e** and **f**) and spleen (**g** and **h**) of untreated (n = 8-10) and IMQ-treated (n = 9) animals. $CD3^+$ and $CD11b^+$ cells are pre-gated on $CD45^+$ population. Representative pseudocolor plots (**e** and **g**) and quantification of populations (**f** and **h**). Data are pooled from 4 independent experiments and shown as mean ± SD (**c** and **d**) or mean (**f** and **h**). Data are analyzed by either Student's t test (two tailed) (**f** and **h**) or Two-Way Anova (**c** and **d**). ns = non-significant, * $p<0.05$, ** $p<0.01$, *** $p<0.001$, **** $p<0.0001$.

Supplementary Figure S2. Toxicity of systemic and topical MTX, MTX-GNP, and GNP therapies in the IMQ-model. (**a** and **c)** Weight changes of different treatment groups in the (**a**) systemic (n = 8-15) and (**c**) topical (n = 7-15) MTX-GNP experiments, calculated as % weight change from pretreatment weight and recorded daily (left), and plotted for day 7 (right)**.** (**b** and **d**) Serum alanine transaminase (ALT) levels from the (**b**) systemic (n = 3-11) and (**d**) topical (n = 6-11) MTX-GNP experiments in the IMQ model. Data are pooled from 3 independent experiments and shown as mean ± SD (**a** and **c)** or mean (**b** and **d**). Data are analyzed by One-Way Anova. ns = non-significant.

Supplementary Figure S3. ^{1}H NMR analysis of systemic bioavailability of topical therapies in the IMQ model. (**a** and **b**) ^{1}H NMR (nuclear magnetic resonance) spectra of samples containing 1 (25 µg/mL, yellow), 10 (250 µg/mL, orange) and 100 doses (2500 µg/mL, blue) of MTX dissolved in D_2O, in order to determine the sensitivity limit. (**a**) The insert shows a zoom on the region around 3.05 ppm that displays a prominent MTX singlet peak. (**b**) The insert shows a zoom on the baseline to display also weak signals. The sensitivity limit for MTX can thus be determined to be 25 µg/ml. (**c**

and **d**) ^{1}H NMR spectra of serum samples from the topical treatment experiments of untreated (green), MTX-GNP (purple), GNP (yellow), or MTX (orange) treated animals and a reference measure (blue) with 100 doses of MTX (**c**) or MTX-GNP (**d**). The asterisk indicates signals stemming for ethanol impurities. (**c**) Both low-field (left) and high-field regions (right) of ^{1}H NMR spectra are displayed. Signals marked with the dashed lines indicate characteristic MTX signals. Evidently, no MTX traces were detected in the investigated samples (sensitivity limit > 25 μg/mL). (**d**) The signal marked with the dashed line indicates a characteristic MTX-GNP signal, which cannot be detected in any of the other samples.

Supplementary Figure S4. Splenic immune landscape in the IMQ model. (**a**) Representative pseudocolor plots depicting the employed gating strategy in order to identify relevant immune subsets in the spleens and ears. Displayed plots are of splenocytes from naïve C57BL/6 mice. (**b-d**) Quantification of $CD45^{+}$ (**b**), $CD3^{+}$ (**c**) and $CD11b^{+}$ (**d**) cell populations in the spleens of mice from the topical treatment experiments on day 7. Quantification of (**e**) αβ and γδ T cell composition of $CD3^{+}$ T cells, (**f**) $CD4^{+}$ and $CD8^{+}$ T cell composition of αβ $CD3^{+}$ T cells and (**g**) $Ly6G^{+}$ and $Ly6G^{-}$ myeloid cell composition of $CD11b^{+}$ cells. n = 9-13 for untreated, n = 9-11 for IMQ-treated, n = 5-7 for topical therapy (MTX, GNP, or MTX-GNP) receiving animals. Data are pooled from 3 independent experiments and shown as mean. Data are analyzed by either One-Way Anova (**b-d**) or Two-Way Anova (**e-g**). ns= non-significant.

Supplementary Figure S5. Histological characterization of patient psoriatic (PP) and healthy-appearing (PN) skin. (**a-c**) Representative H&E (**a**) and immunofluorescence staining (**b** and **c**) of psoriatic (PP) (**a** left and **b**) and normal-appearing (PN) (**a** right and **c**) skin biopsies taken from a psoriasis patient (n = 3). (**a**) Scale bar = 200μm. (**b** and **c**) Left, CD45 (green, arrowhead), IL-17 (magenta, asterisk), and DAPI (blue). Right, CD3 (green, arrowhead), Foxp3 (magenta, asterisk), CD8 (red, arrow), and DAPI (blue). Scale bar = 100μm (top), and 50μm (bottom). (**d**) Representative H&E staining of PN skin (left), skin grafts harvested on day 21 (middle) and day 35 (right). Scale bar

= 100µm. (**e**) Quantification of acanthosis (left) and papillomatosis index (middle) and total T cell counts (right) on day 0 (n = 2), day 21 (n = 6) and day 35 upon Vaseline (n = 5-6, black open circles), TCB (n = 5-6, blue open circles), or MTX-GNP (n = 5-6, purple open circles) treatments. Data are shown as mean ± SEM.

Supplementary Figure S6. Transcriptomic changes of the psoriatic human skin and graft upon TCB and MTX-GNP treatment. (**a**) Gene expression differences between the PP versus PN skin biopsies. (**b**) Differentially expressed genes (DEGs) between the PP and PN skin biopsies, from the selected gene sets of cytokines and chemokines. (**c-d**) Gene expression differences between the MTX-GNP versus Vaseline (**c**) and TCB versus Vaseline (**d**) treated human skin grafts from the AGR experiments. (**e**) Regulation of known target genes of TCB treatment. (**f**) RT-PCR evaluation of Il17a mRNA expression in the post-transplantation AGR skin from Vaseline, TCB, and MTX-GNP treatment groups (n = 2, per treatment group). Data in (**f**) are analyzed by One-Way Anova.

SUPPLEMENTARY METHODS

Quantitative Real-Time PCR (RT-PCR): complementary DNA (cDNA) remaining from the RNA sequencing was used for quantitative Real-Time PCR analysis Il17a expression. RT PCR was performed as previously published (Bouchaud et al., 2013). Briefly a 3-minute denaturation step at 95°C was followed by 40 cycles at 95°C for 5 seconds and 60°C for 30 seconds. A final dissociation stage was carried out at 95°C for 5 seconds and 60°C for 30 seconds. *Rps29* was used as a house-keeping gene, and the expression of *Il17a* was normalized to the expression of *Rps29* within the same sample. Genes of interest were amplified using the following primers:

Rps29 Forward: 5`-CGC TCT TGT CGT GTC TGT TCA-3'

Rps29 Reverse: 5`-CCT TCG CGT ACT GAC GGA AA-3'

Il17a Forward: 5`-CAA TCC CAC GAA ATC CAG GAT G-3'

Il17a Reverse: 5`-GGT GGA GAT TCC AAG GTG AGG-3'

^{1}H NMR: ^{1}H NMR spectra were detected on a 600 MHz (14.1 T) Bruker HDIII NMR spectrometer (USA) equipped with a TXI Z-gradient probe operating at 298 K. Sample volumes of 250 μL were loaded in Shigemi-type sample tubes as optimized for proton detection. All samples either contained 10% v/v D_2O (for serum measurements) as lock-solvent or were dissolved in pure D_2O (for MTX titration). Free induction decays were recorded by averaging 256 detections with 90˚ pulses, each after a Watergate sequence (Rule and Hitchens, 2006) that suppresses the water resonance using a 10 ms long PC9 shaped pulse. The carrier frequency was set to 4.7 ppm. Data were processed using NMRpipe (Delaglio et al., 1995) and home-written MATLAB scripts. All FIDs were apodized and zero-filled prior to Fourier transformation.

REFERENCES

Bouchaud G, Gehrke S, Krieg C, Kolios A, Hafner J, Navarini AA, et al. Epidermal IL-15Ralpha acts as an endogenous antagonist of psoriasiform inflammation in mouse and man. J Exp Med 2013;210(10):2105-17.

Delaglio F, Grzesiek S, Vuister GW, Zhu G, Pfeifer J, Bax A. Nmrpipe - a Multidimensional Spectral Processing System Based on Unix Pipes. J Biomol Nmr 1995;6(3):277-93.

Rule GS, Hitchens TK. Fundamentals of Protein NMR Spectroscopy. Dordrecht: Springer, 2006.

Table S1: Antibodies used for Flow Cytometry:

Antibody	Fluorophore	Supplier	Clone	Catalog No
anti-mouse CD3	BV510	BD	145-2C11	563024
anti-mouse CD45.2	FITC	invitrogen	1O4	11-0454-82
anti-mouse CD8b	APC-eFluor780	invitrogen	H35-17.2	47-0083-82
anti-mouse CD4	Percp-Cyanine5.5	invitrogen	RM4-5	45-0042-82
anti-mouse Ly6G	BV711	Biolegend	1A8	127643
anti-mouse CD11b	BV650	Biolegend	M1/70	101239
anti-mouse Ki67	PE-Cyanine7	invitrogen	SolA15	25-5698-80
anti-mouse γδ TCR	eFluor450	invitrogen	eBioGL3	48-5711-82
anti-human CD3	BV785	Biolegend	UCHT1	300401
anti-human CD4	BUV395	BD	SK3	563550
anti-human CD8	BV510	Biolegend	RPA-T8	301047

Table S2: Antibodies used for Immunofluorescence:

Antibody	Fluorophore	Supplier	Clone	Catalog No
anti-mouse CD45.2	AlexaFluor488	Biolegend	1O4	109816
anti-mouse/human IL-17	unconjugated	Abcam	polyclonal	ab79056
anti-human CD45	AlexaFluor488	Biolegend	2D1	304019
anti-human CD3	AlexaFluor488	Biolegend	UCHT1	300454
anti-human CD8	AlexaFluor647	Biolegend	SK1	344726
anti-human Foxp3	eFluor570	invitrogen	236A/E7	41-4777-82

Supplementary Figure 1

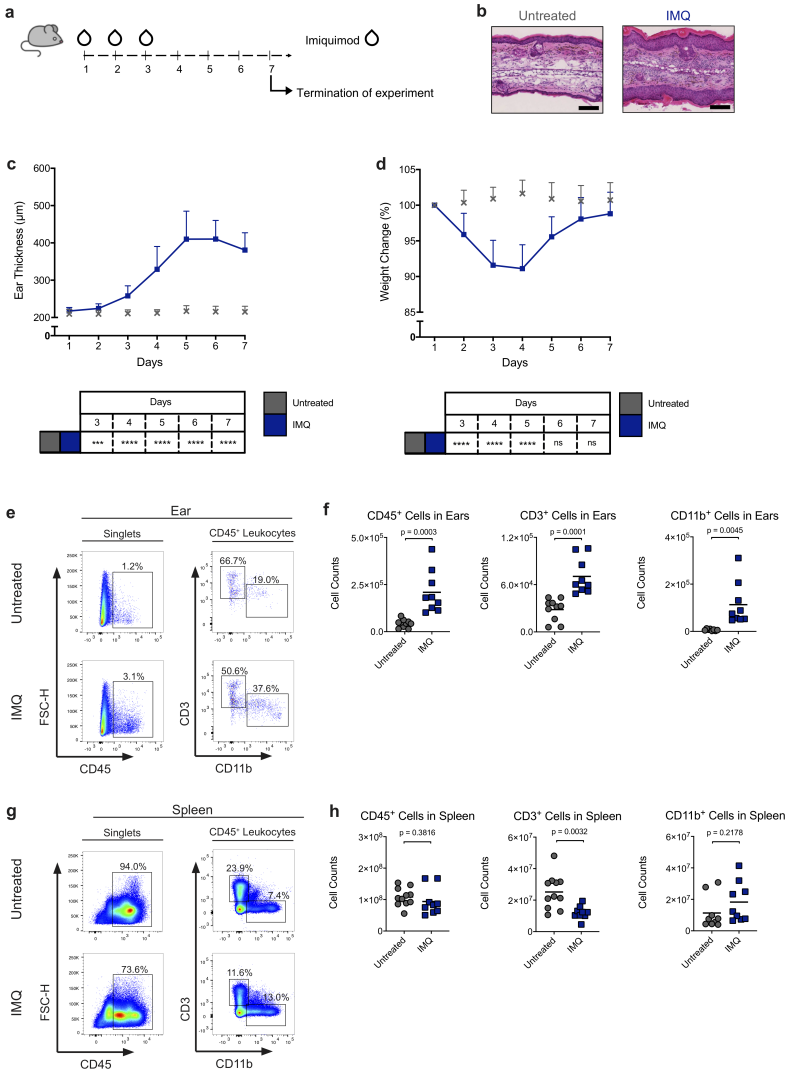

Supplementary Figure 2

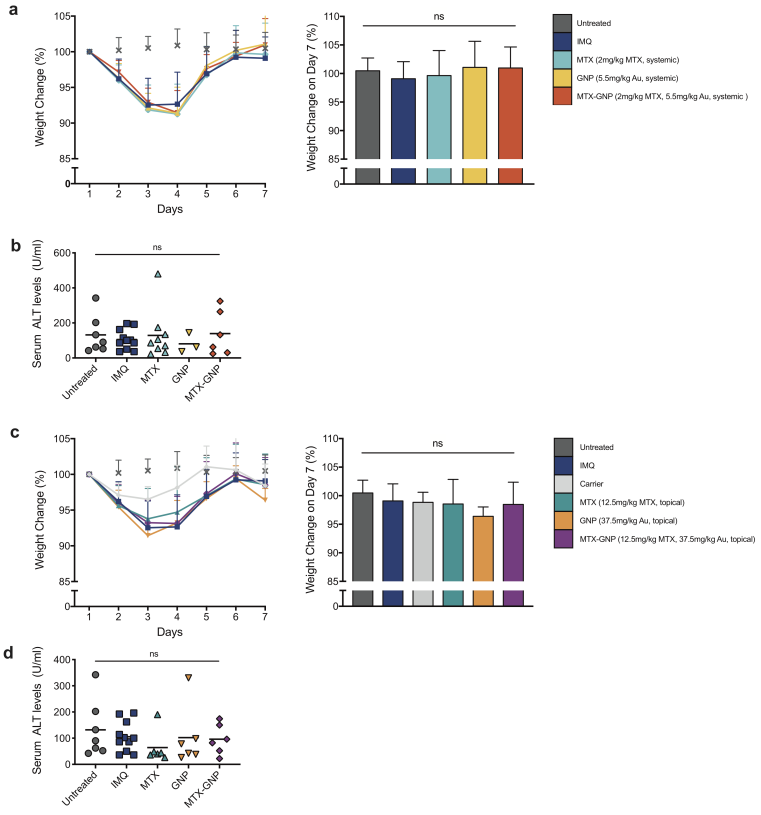

Supplementary Figure 3

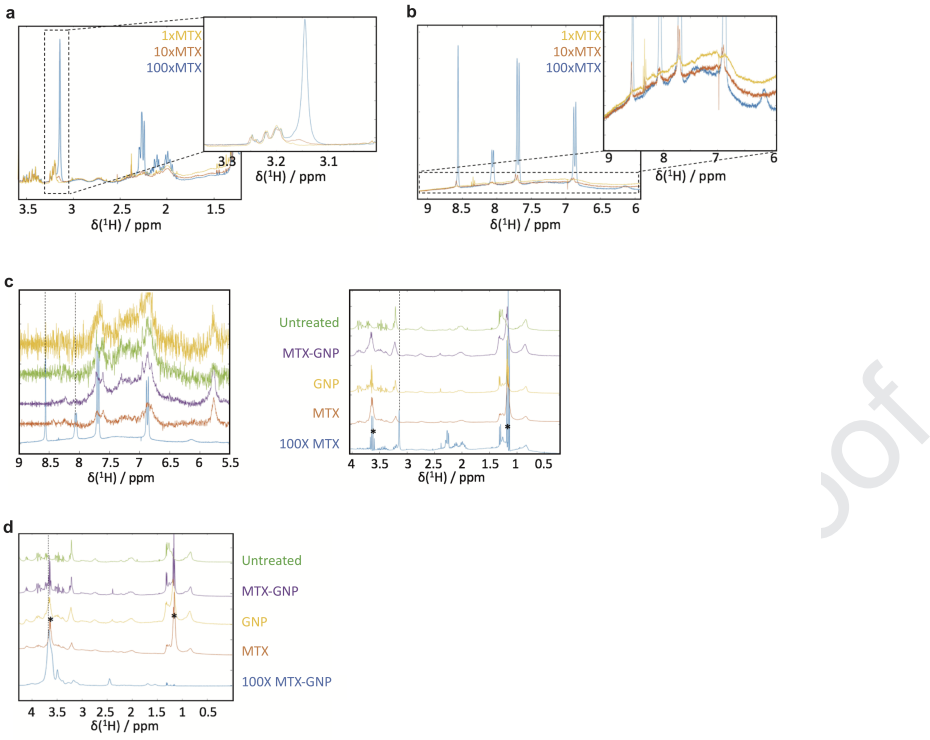

Supplementary Figure 4

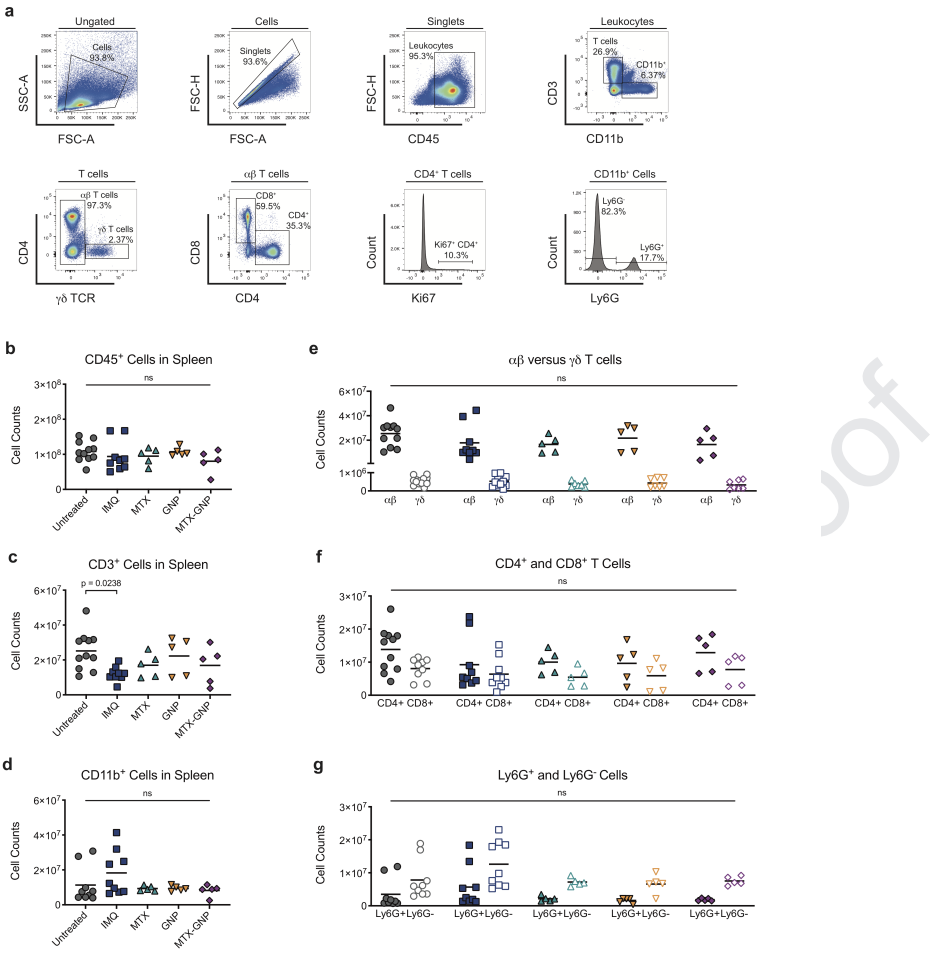

Supplementary Figure 5

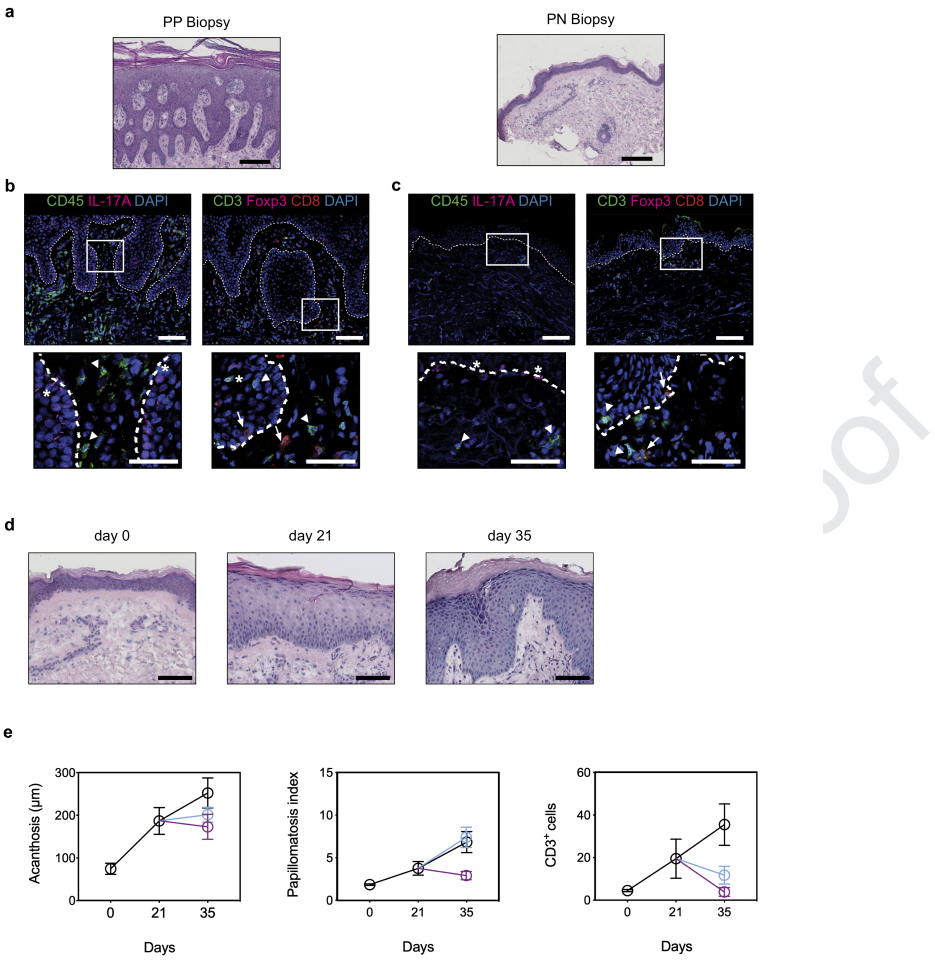

Supplementary Figure 6